

Breaking of scale invariance in a strongly dipolar 2D Bose gas

Haoting Zhen,^{1,*} Yifei He,^{1,*} Sampriti Saha,² Mithilesh K. Parit,¹
Mingchen Huang,¹ Nicolò Defenu,² and Gyu-Boong Jo^{3,4,1,†}

¹*Department of Physics, The Hong Kong University of Science and Technology, Clear Water Bay, Kowloon, Hong Kong*

²*Institut für Theoretische Physik, ETH Zürich, Wolfgang-Pauli-Str. 27 Zürich, Switzerland.*

³*Department of Physics and Astronomy, Rice University, Houston, TX, USA*

⁴*Smalley-Curl Institute, Rice University, Houston, TX, USA*

(Dated: October 27, 2025)

Two-dimensional (2D) dipolar atomic gases present unique opportunities for exploring novel quantum phases due to their anisotropic and long-range interactions. However, the behavior of strongly dipolar Bose gases in 2D remains unclear, especially when dipoles are tilted. Here, we demonstrate the creation and characterization of strongly dipolar 2D condensates in a quasi-2D harmonic trap with tunable dipole orientation. By investigating scale invariance properties through breathing collective mode measurements, we observe significant breaking of scale invariance when dipoles are tilted in-plane indicating the dominance of the nonlocal dipole-dipole interactions (DDIs) in this regime. Interestingly, the breaking of the scale invariant dynamics is accompanied by an increase in quantum fluctuations, as shown by comparison with mean-field and beyond mean-field theoretical studies. Our experiments also reveal that at critical tilt angles around 70°, stripe-type density modulations emerge, suggesting the presence of a roton spectrum in 2D, while the system still shows hydrodynamic nature with the phase-locking breathing behavior. This observation elucidates the many-body effect induced by DDIs in 2D, thus marking a crucial step toward realizing 2D supersolids and other exotic quantum phases.

Two-dimensional (2D) bosons with dipole-dipole interactions (DDI) involve both isotropic short-range and anisotropic long-range interactions. In contrast to 2D Bose gases with contact interactions only - where the interaction-induced Berezinskii-Kosterlitz-Thouless (BKT) mechanism [1–3] reveals superfluidity with quasi-long-range order [4–6] - the DDI stabilizes various crystalline structures, potentially leading to the emergence of supersolid order. While interesting scenarios can occur when dipoles are tilted, a systematic understanding of strongly dipolar 2D systems remains elusive, especially how crystalline structure emerges with superfluidity. In this work, we take advantage of the scale invariance, a fundamental property resulting from length-scale-free short-range interaction in 2D, and examine how strong DDI breaks such invariant property [6–9] and manifests itself in the 2D superfluid [10].

Recently, a single-layer quasi-2D dipolar superfluid with tunable dipolar angles was realized with moderate DDIs $\epsilon_{dd} \sim 0.5$ [11] (where $\epsilon_{dd} = a_{dd}/a_s$ represents the ratio of dipolar to contact scattering lengths). While mild anisotropic effects of DDIs manifest in density fluctuations for tilted dipoles, an effective contact-like treatment of DDIs sufficiently describes the BKT superfluid transition, and scale-invariant behavior is observed from equations of state. Nonetheless, DDIs are expected to produce more pronounced effects in the strongly dipolar regime with $\epsilon_{dd} \gtrsim 1$ in 2D, where intriguing phenomena such as anisotropic superfluidity [12], anisotropic vortex cores [13], anisotropic vortex-vortex interactions [14], and

2D stable bright solitons [15, 16] are predicted.

Another open question is the possible existence of supersolid in 2D [17] when density modulation induced by roton instability [18] coexist with 2D superfluidity. As a phase with crystalline structure and global phase coherence, supersolid has been observed in elongated or oblate dipolar gases in 3D [19–23]. In 2D, complex supersolid phases are expected to be found in a strongly dipolar gas with perpendicular dipoles at zero temperature [24–27], though the required density is far higher than current experimental capability. Recently, several works found that a strongly dipolar 2D gas with tilted dipoles can potentially host a stripe-like supersolid with much lower density [28–33], which coincides with the solid-like density modulations observed in the strongly dipolar gas trapped in a quasi-2D pancake trap [34]. In the same setup, however, no experimental evidence of phase coherence could be found. This is in agreement with the theoretical picture in Refs. [35, 36], where the thermodynamic stability of 2D supersolid has been questioned.

Here, we produce strongly dipolar 2D condensates in a quasi-2D harmonic trap with variable dipole orientation. We examine the scale invariance properties with DDIs by measuring the breathing mode. A strong breaking of scale invariance is observed when dipoles are tilted in plane, indicating the dominance of the nonlocal interaction involved with $1/r^3$ scaling of dipole interactions. By increasing ϵ_{dd} over 1, we find the breathing mode frequency displays a larger up-shift and observe a stripe-type density modulation with tilt angle at 70°, which suggest the softening of the roton excitations in the 2D spectrum. Lastly, we study the phase-locking behavior of the breathing mode, validating the nature of our strongly dipolar 2D condensates.

* These authors contributed equally.

† email: gbj@rice.edu

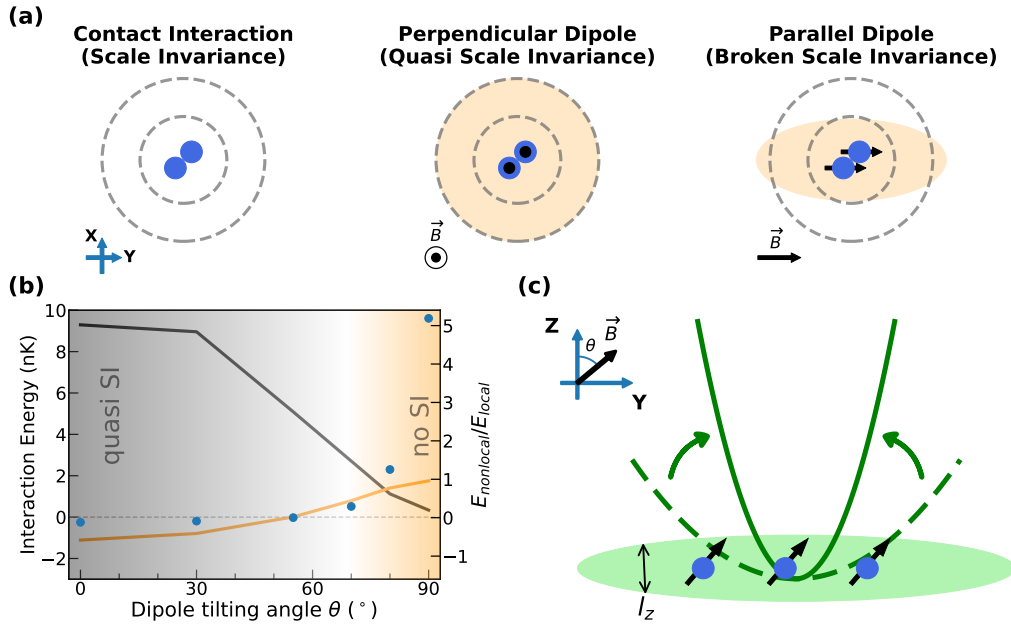


FIG. 1. Scale-invariance theory and the breathing mode in a quasi-2D dipolar gas. **a**, Breaking of scale invariance (SI) in a quasi-2D dipolar gas. At the classical field level, isotropic contact interactions preserve SI due to their short-range nature. When dipoles are aligned perpendicular to the 2D plane, DDIs (shown in yellow) are largely isotropic and short-range, resulting a quasi-scale-invariance (quasi-SI). In contrast, SI is broken when dipoles lie parallel to the 2D plane, where local interactions are suppressed and the anisotropic nonlocal part of the DDIs become significant. **b**, Energy contributions from local contact interactions and nonlocal DDIs as a function of dipole angle θ with $\epsilon_{dd} = 0.98$. The black and orange solid lines represent the local and nonlocal interaction energies, respectively, computed from a simulated ground-state profile (see text). Dots indicate the ratio $E_{\text{nonlocal}}/E_{\text{local}}$. Shaded regions and the dashed line serve as visual guides. **c**, Experimental setup. A sheet beam tightly confines atoms along the z-axis, with an oscillator length $l_z \sim 0.24\mu\text{m}$. An external magnetic field \vec{B} , rotating in the y-z plane, controls the dipole orientation. A quench of the radial trap excites the breathing mode in the x-y plane.

The collective modes we use in this work are fundamental properties for understanding a many-body state, which is associated with the low-lying excitation of quantum gases. In particular, the breathing mode is a sensitive probe of collective properties such as interaction [37, 38] and correlation [39], it has been extensively used to characterize different physical processes such as dimensional crossover [40–43] and phase transitions [44–49]. In an elongated dipolar gas, the lowest-lying collective mode is used to manifest the simultaneous breaking of the phase invariance and the translational symmetry, which establishes the supersolid nature in the sample [46]. Here, we utilize this powerful tool to explore the competition between local and nonlocal interactions in a strongly dipolar 2D superfluid, which provides valuable insights on the distinctive nature of different phases of matter existing in 2D dipolar gas.

NON-LOCAL PART OF DDI AND SCALE INVARIANCE

For a 2D Bose gas with only contact interactions, the ratio between breathing mode frequency and trap frequency in 2D exhibits a universal value $\omega_B/\omega_t = 2$, and the interaction dependence to the breathing mode fre-

quency, which is caused only by quantum fluctuations, is negligible [50–53]. This universal property stems from the $SO(2, 1)$ symmetry, which arises from the reduction of the conformal invariance of the homogeneous gas by the parabolic trapping potential [54]. In Bose gases, typical interaction strengths are not strong enough to observe this correction [7], but observations of quantum scale anomaly [55] (see Methods) have been reported in strongly-interacting 2D Fermi gases [42, 43].

For quasi-2D dipolar gases where atoms occupy the ground state of the axial harmonic confinement, interactions can be considered as a combination of a contact-like part and a nonlocal part [58]. The former $E_{\text{local}} \propto \tilde{g}_{\text{eff}} \int n(r)^2 dr^2$ describes the contribution of contact interaction and the local part of DDI, where the effective interaction strength $\tilde{g}_{\text{eff}} \propto a_{\text{eff}}/l_z = (a_s + a_{dd}(3 \cos^2 \theta - 1))/l_z$ is dimensionless. Thus, the value \tilde{g}_{eff} is determined by both the 3D s-wave scattering length a_s and the dipolar length $a_{dd} = \mu_0 \mu_m^2 m / 12\pi\hbar^2$ in units of the transverse oscillator length $l_z = \sqrt{\hbar/m\omega_z}$, which confines the atoms to the 2D plane. θ is the angle between the dipoles and the z axis. The nonlocal part of DDIs can be expressed

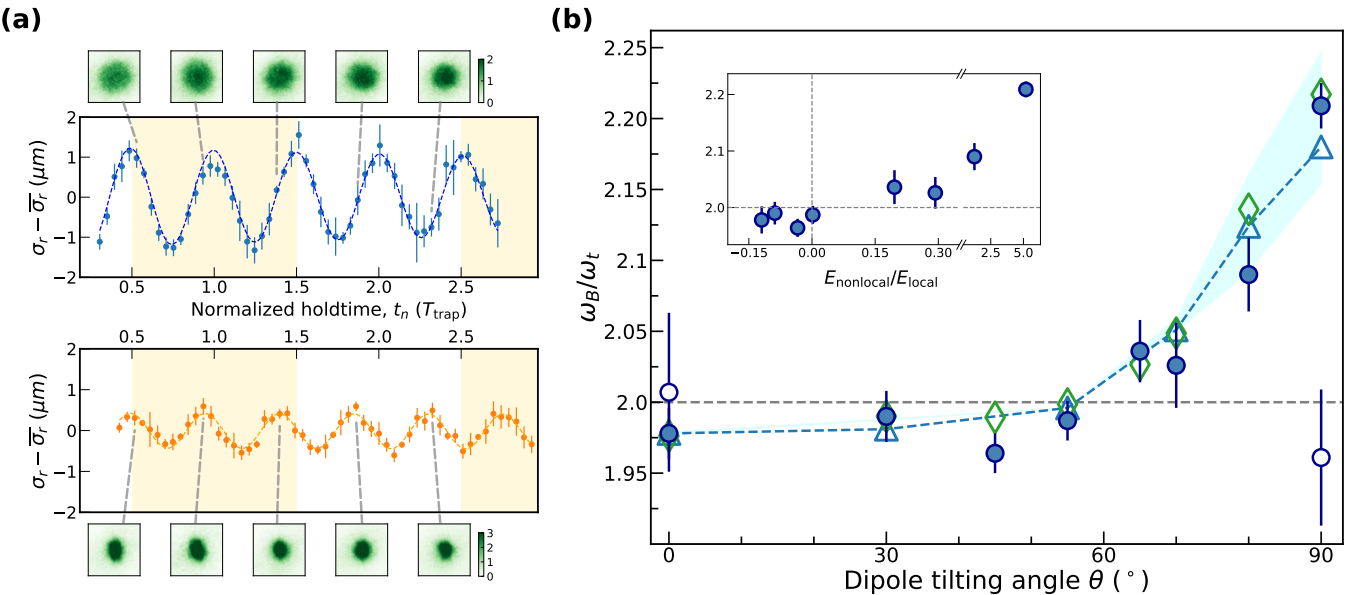


FIG. 2. Breaking of scale invariance in coherent dipolar samples with tilted dipole orientation θ . **a**, Example measurements of the breathing mode dynamics. Top and bottom panels show in-situ images for $\theta = 0^\circ$ and 90° samples, respectively, at $\epsilon_{dd} = 0.98$, displayed as the optical density. Central panels depict oscillations in the average radial width σ_r , plotted relative to its mean value over all hold times, $\bar{\sigma}_r$. The holdtime t_n is normalized by the trap period T_{trap} . Dashed lines are damped sinusoidal fits [56]. The shades representing one trap period are guides to eyes. **b**, The breathing frequency of a quasi-2D dipolar gas with $\epsilon_{dd} = 0.98$ and different dipole orientations. The blue (white) points correspond to the breathing mode frequencies of condensates (normal gas). As dipoles rotate into the 2D plane, the breathing mode frequency of the condensates gradually deviates from the $SO(2, 1)$ symmetry value $\omega_B = 2\omega_t$, represented by the grey dashed line. The mean-field GPE simulation is shown as triangles, and the blue dashed lines are direct connection of the symbols. The results of the MCTDHB simulation with $M = 2$ are shown as green open diamonds. Incorporating quantum fluctuations does not significantly alter the GPE predictions, except at large θ , where quantum effects shift the frequency upward, in agreement with experimental observations. The blue shade represents the calibration uncertainty on a_s [57]. The inset compares the breathing mode frequency to the relative strength of nonlocal DDIs. Error bars represent the 95% confidence interval.

by [12],

$$E_{\text{nonlocal}} \propto \tilde{g}_{dd} \int d\mathbf{r}^2 n(\mathbf{r}) \int \frac{d\mathbf{k}^2}{(2\pi)^2} e^{i\mathbf{k}\cdot\mathbf{r}} F_d \left(\frac{kl_z}{\sqrt{2}} \right) n(\mathbf{k}), \quad (1)$$

$$F_d(x) = xe^{x^2} \text{erfc}(x) (-\cos^2 \theta + \sin^2 \theta \cos^2 \phi_k), \quad (2)$$

where $\tilde{g}_{dd} \propto a_{dd}/l_z$ is the effective 2D coupling strength of DDIs, erfc is the complementary error function, and ϕ_k is the angle between \mathbf{k} and the projection of dipole orientation on the 2D plane. The kernel F_d captures the long-range nature of DDIs in quasi-2D, as it is explicitly dependent on the magnitude of the momentum \mathbf{k} . While E_{local} preserves scale invariance, E_{nonlocal} does not, as it can be confirmed by inspecting the isotropic case. For $\varphi_k \approx 0$, the function $F_d(x)$ becomes flat at large momenta $k \gg l_z$ while behaving linearly for $k \lesssim l_z$. Thus, the two momentum region transform differently with $k \rightarrow k/\lambda$, and scale invariance is broken.

In a quasi-2D dipolar gas, E_{nonlocal} typically becomes small compared to E_{local} due to the relatively large effective local interaction strength \tilde{g}_{eff} [59]. In this case, the contribution of nonlocal DDIs can be neglected and the scale invariance is largely preserved, which is observed in 2D Townes solitons [60] and 2D dipolar superfluid [11]. While stronger nonlocal DDIs can be found in systems

with larger dipole moments such as polar molecules [61], it can produce significant effects in weaker dipolar systems if local interactions are strongly suppressed. Such suppression can be achieved by either decreasing a_s via Feshbach resonance or tilting dipoles into the 2D plane, as reflected in the form of $\tilde{g}_{\text{eff}} \propto (a_s + a_{dd}(3\cos^2 \theta - 1))$. A schematic of this effect is shown in Fig. 1a. The scale invariance is largely preserved in a 2D dipolar gas with out-of-plane dipoles where local interactions dominate. Only with dipoles tilted in-plane, the anisotropic nonlocal DDIs significantly alter the scaling dynamics of the system. This effect can be visualized by the computation of the interaction energies from both local and non-local DDIs based on a simulated ground-state density profile [56]. As shown in Fig. 1b, as θ increases, nonlocal interactions gradually dominate, driving the system into the scale invariance-breaking regime.

BREAKING OF SCALE INVARIANCE WITH TILTED DIPOLES

To investigate scale invariance in presence of DDIs, we perform our experiments employing a spin-polarized gas of ^{166}Er , which is loaded into a quasi-2D trap and probe breathing mode oscillation frequency ω_B in the strongly

dipolar regime with $\epsilon_{dd} \gtrsim 1$ (see Methods for more details). Here, the angle θ serves as a control parameter to investigate how gas dynamics evolves as scale invariance is progressively broken. To compare ω_B with the standard value of $2\omega_t$, we determine the radial trap frequency using dipole modes simultaneously excited by the same quench. By performing a sinusoidal fit to the oscillation of the cloud center, we obtain the trap frequencies ω_x and ω_y along the two trap principal axes [56]. The mean trap frequency is calculated as $\omega_t = \sqrt{\omega_x \omega_y}$.

Fig. 2a shows an example measurement of the breathing mode. The top and bottom panels display the in-situ density profiles of the sample with $\theta = 0^\circ$ and $\theta = 90^\circ$, respectively, imaged at different hold times. The sample with $\theta = 90^\circ$ appears smaller and denser due to the reduction in repulsive local interactions [11]. At the five selected hold times, the $\theta = 90^\circ$ sample is maximally expanded, whereas the $\theta = 0^\circ$ sample contracts from its maximum width to the minimum. This contrast is reflected in the oscillations of σ_r for both angles, as shown in the central panels. After normalizing the hold time t by the trap period $2\pi/\omega_t$, we observe that the sample with $\theta = 90^\circ$ oscillates significantly faster than that with $\theta = 0^\circ$, indicating a breaking of scale invariance.

Unlike the case of local interactions, where such violations typically arise from quantum fluctuations [55], here the breakdown occurs already at the semi-classical level due to the $\propto r^{-3}$ scaling of dipolar interactions. To systematically explore the impact of DDIs, we measure the breathing mode frequency across a range of dipole tilt angles, $\theta = 0^\circ, 30^\circ, 45^\circ, 55^\circ, 65^\circ, 70^\circ, 80^\circ$, and 90° , while keeping the dipolar strength fixed at $\epsilon_{dd} = 0.98$. As shown in Fig. 2b, the ratio ω_B/ω_t remains close to 2 when the dipoles are predominantly oriented out-of-plane. In this regime, local interactions dominate over nonlocal contributions, maintaining quasi-scale invariance with $E_{\text{interaction}} \approx E_{\text{local}}$. As the dipoles are tilted further into the plane, the nonlocal component of the DDIs becomes increasingly significant, leading to a marked upshift in ω_B/ω_t . Here, the contact interaction and the local part of the DDIs nearly cancel, resulting in an effective local interaction strength \tilde{g}_{eff} approaching zero. Consequently, the residual nonlocal interactions govern the system's behavior. The most pronounced deviation occurs at $\theta = 90^\circ$, where ω_B/ω_t exceeds the standard value of 2 by approximately 10%, signaling a strong violation of scale invariance.

We also measure the breathing mode frequency of two samples in the non-condensate regime, with dipoles oriented perpendicular to and within the 2D plane. These samples are prepared with a lower atom number $N \approx 1.9 \times 10^4$, and a higher temperature $T \approx 1.6\hbar\omega_z$. As shown in Fig. 2b, ω_B/ω_t recovers the standard value of 2 within experimental resolution. No significant up-shift is observed with $\theta = 90^\circ$, indicating that quasi-scale invariance persists in the strongly dipolar 2D thermal gas, independent of dipole orientation. This result already points to the deep connection between the breaking of scale in-

variance and the emergence of strong quantum fluctuations. In the thermal regime, quantum correlations are weak, rendering the contribution of nonlocal interactions also negligible [62], see the inset Fig. 2b. This measurement also demonstrates that the frequency of collective oscillation could serve as a probe for identifying the superfluid phase in a strongly dipolar 2D gas within the scale invariance-breaking regime.

The connection between quantum coherence in the 2D gas and the violation of $SO(2, 1)$ symmetry highlights a subtle interplay between the long-range tails of the dipolar interaction—which explicitly break the $SO(2, 1)$ invariance—and the quantum fluctuations inherent to the system. It is crucial to disentangle the effects of scale invariance breaking that emerge at the semi-classical level, from those—if present—that stem from the interplay between the dimensional nature of dipolar interactions and the many-body correlations within the gas.

To investigate this interplay, we adopt a multi-configurational time-dependent Hartree for bosons (MCTDHB) framework accounting quantum fluctuations [63, 64] as well as a time-dependent Gross-Pitaevskii equation (GPE) solver at the semiclassical level [56] to simulate the breathing mode dynamics of samples at various tilt angles θ . In general, the semiclassical results (empty triangles) show good match with experimental measurements (full circles), except that a significant upward shift is observed in both experimental data and MCTDHB at $\theta = 90^\circ$, as illustrated in Fig. 2b. This upward shift from the semiclassical prediction, observed at $\theta = 90^\circ$, implies the effect of quantum fluctuation, which is accounted in the MCTDHB simulation with $M = 2$ orbitals. A similar shift has been studied theoretically in 3D contact gas [65]. Interestingly, the most pronounced effect from quantum fluctuations coincides with the strongest breaking of scale-invariance at the semiclassical level.

In the inset of Fig. 2b, we plot ω_B/ω_t with respect to the relative strength of nonlocal and local interactions, showing a clear relationship between the $SO(2, 1)$ symmetry violation and the dominance of nonlocal DDIs. Interestingly, from both the GPE simulation and the MCTDHB simulation, we find that a negative nonlocal interaction energy leads to a down-shift in ω_B/ω_t relative to 2, while a positive nonlocal interaction energy causes an up-shift. Experimentally, it should be noticed that the down-shift below 55° may arise from a combination of third-dimensional effects [40] and the negative nonlocal interaction energy.

TOWARD THE STRONGLY DIPOLAR REGIME

Since the violation of $SO(2, 1)$ symmetry arises from the non-local part of DDIs, the breathing mode frequency effectively characterizes the strongly dipolar regime where more significant violations occur when $\epsilon_{dd} > 1$. To study the breathing mode in this regime,

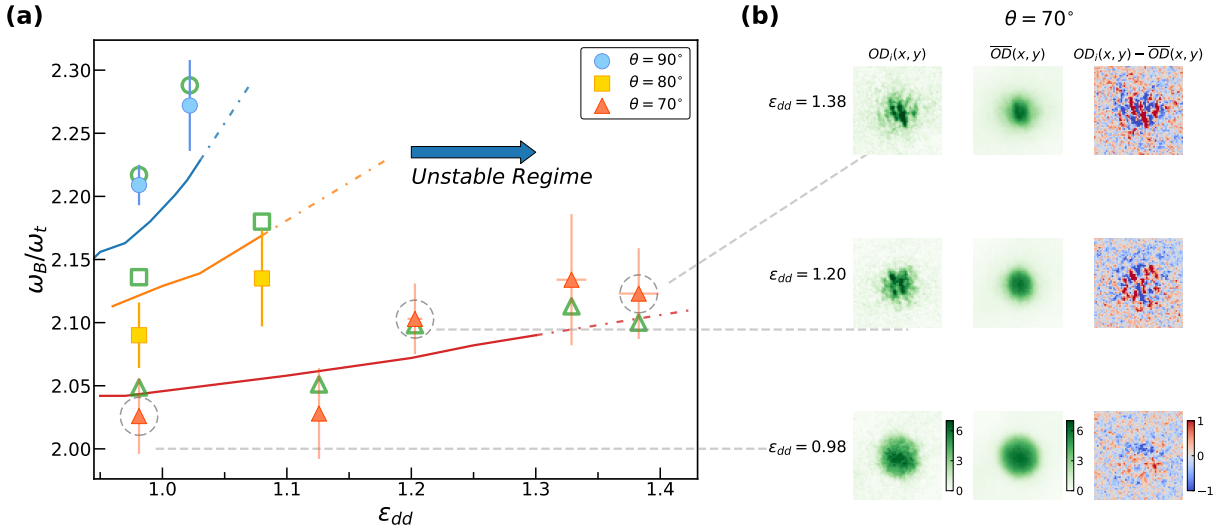


FIG. 3. **The signatures of nonlocal DDIs in the strongly dipolar regime.** **a**, The breathing mode frequency of samples in the strongly dipolar regime with highly tilted dipoles. With larger ϵ_{dd} , ω_B deviates more from the standard value. While the mean-field GPE simulation, plotted as solid lines (and the dash-dot line as extension in the mean-field unstable regime), captures the trend of this strong scaling anomaly, the MCTDHB simulation, shown as green labels, matches the measurements better by including the effect of quantum fluctuations. Error bars represent the 95% confidence interval. **b**, The in-situ profiles of samples with $\theta = 70^\circ$ and $\epsilon_{dd} = 0.98, 1.20, 1.38$. Three example single images $OD_i(x, y)$ are shown in the left column, plotted in the optical density (OD). The corresponding profiles $OD(x, y)$ are shown in the middle column. The right column shows the contrast between $OD_i(x, y)$ and $\overline{OD}(x, y)$, visualizing the emergence of the stripe-like density modulation in the roton-unstable regime.

we tuned ϵ_{dd} by adjusting a_s via Feshbach resonance. As shown in Fig. 3a, an enhanced up-shift of the breathing mode frequency ω_B is observed with increasing ϵ_{dd} . The degree of this enhancement depends on the dipole orientation and reaches a maximum at $\theta = 90^\circ$, which can be explained by the corresponding reduction in the effective local interaction strength \tilde{g}_{eff} , thus enhancing the role of the nonlocal DDIs.

Fig. 3a summarizes the measured breathing oscillation frequencies alongside GPE and MCTDHB theoretical predictions. Discrepancies between GPE and MCTDHB become increasingly significant when approaching the unstable regime. Compared to the GPE results, which is plotted as solid lines, the MCTDHB analysis generally improves the quantitative accuracy by shifting the predicted frequencies upward. This correction is already noticeable at $\theta = 70^\circ$ for $\epsilon_{dd} \geq 1.2$, and becomes essential to reconcile theory with experiment at $\theta = 90^\circ$. $\theta = 90^\circ$ could be an ideal condition to further investigate the effect of quantum fluctuations in the 2D regime. As expected, the GPE simulations break down in the regime where both θ and ϵ_{dd} are high enough for the system becomes unstable without the beyond-mean-field contribution, which stabilizes the gas against the instability induced by attractive DDIs [66]. We measure ω_B of two samples within this mean-field unstable regime, with $\theta = 70^\circ$ and $\epsilon_{dd} = 1.33, 1.38$. The results continue to show a deviation from the expected $SO(2, 1)$ symmetry value. Notably, the MCTDHB simulation with $M = 2$ remains stable at higher values of ϵ_{dd} with respect to the GPE, providing a reliable theoretical estimate for

the breathing mode frequency that aligns well with experimental observations. The breathing frequency of the sample with $\theta = 80^\circ$ is slightly down-shifted from both the MCTDHB and GPE simulation, which we attribute to the larger quench amplitude employed in the measurement [67].

At large ϵ_{dd} , stripes patterns also emerge in the experimental sample, as presented in Fig. 3b. The density fluctuations become more pronounced with increasing ϵ_{dd} and manifests as a stripe-like modulation aligned with the dipole orientation within the 2D plane. In particular, \tilde{g}_{eff} remains small yet positive in this regime, indicating that the instability does not stem from a global collapse due to the attractive isotropic local interactions. Instead, this modulational instability is likely associated with the predicted emergence of a roton instability [28]. Such roton-like instability is a hallmark of the anisotropic non-locality of DDIs in a strongly confined dipolar gas [18].

CHARACTERIZING 2D STRONGLY DIPOLAR BOSE GASES

In previous work [11], quasi-long-range coherence associated with BKT superfluid was observed in a 2D dipolar system with moderate $\epsilon_{dd} \sim 0.5$ and tilted dipole angles. Here, we demonstrate that the strongly dipolar sample exhibits hydrodynamic behavior at low temperature but becomes collisionless at higher temperature. We investigate the anisotropy of the breathing frequencies $\delta_B = |\omega_{bx}/\omega_{by} - 1|$, where ω_{bx} and ω_{by} denote the oscillation frequencies along the x and y directions, respectively. The corresponding frequency ratio ω_B/ω_t is plotted in Fig. 4a for the three dipole orientations. The data points are extracted from the in-situ images and the error bars represent the 95% confidence interval. The MCTDHB simulation (green circles) matches the experimental data (green symbols with error bars) better than the GPE simulation (solid lines). The frequency ratio ω_B/ω_t increases with ϵ_{dd} and reaches a maximum at $\theta = 90^\circ$ for $\epsilon_{dd} \geq 1.2$. The frequency ratio ω_B/ω_t is also plotted in Fig. 4b for the three dipole orientations. The data points are extracted from the in-situ images and the error bars represent the 95% confidence interval. The MCTDHB simulation (green circles) matches the experimental data (green symbols with error bars) better than the GPE simulation (solid lines). The frequency ratio ω_B/ω_t increases with ϵ_{dd} and reaches a maximum at $\theta = 90^\circ$ for $\epsilon_{dd} \geq 1.2$.

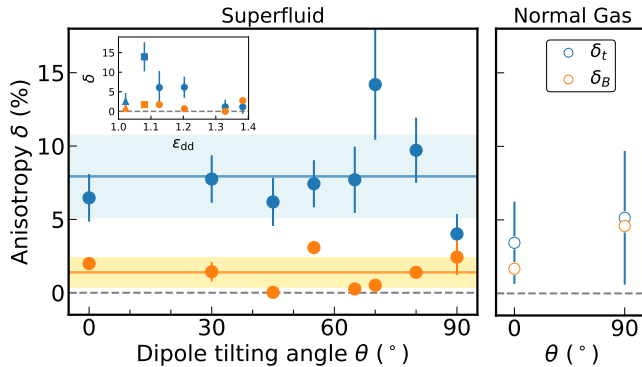


FIG. 4. Anisotropy of the breathing mode in the hydrodynamics and collisionless regime. The anisotropy of breathing mode δ_B and the trap frequency anisotropy δ_T of samples with $\epsilon_{dd} = 0.98$ and different dipole angles are shown in orange and blue points. The left (right) panel demonstrates the condensate (normal gas) sample. The blue (orange) solid lines and shades represent the mean and the standard deviation of the trap (breathing) anisotropy. The dashed line is a guide to eyes. Error bars represent the 95% confidence interval. The inset shows the data of samples with $\epsilon_{dd} > 1$ and dipole angles at 70° (circles), 80° (squares) and 90° (triangles).

tion frequencies of σ_x and σ_y , respectively. In weakly interacting condensates or strongly interacting normal gases, the breathing mode exhibits the phase-locking oscillation, i.e., $\delta_B \approx 0$, as described by hydrodynamic theory [41, 68]. This signature of hydrodynamic nature, previously observed in 2D Fermi gases [42, 52], is also clearly present in our superfluid samples as shown in Fig. 4. Despite significant trap anisotropy δ_T , the measured δ_B in the condensate remains close to 0 and shows no correlation with δ_T or dipole orientation. These findings suggest the superfluid nature of our samples, even when \tilde{g}_{eff} is small at large θ . In contrast, samples in the normal gas regime exhibit finite breathing anisotropy comparable to the trap anisotropy, consistent with decoupled oscillations along two directions in the collisionless limit [52].

OUTLOOK AND CONCLUSION

With tilting dipoles, we observe the breaking of scale invariance in coherent quasi-2D strongly dipolar gases, which is a result from the dominance of nonlocal interaction over local interaction. While the phase-locking behavior of the breathing mode reflects the superfluid hydrodynamics nature of the samples, the emergent stripe-type density modulations in the unstable regime indicate the onset of roton, possibly providing a precursor of a 2D stripe supersolid [31, 32].

We show that the explicit breaking of the $SO(2,1)$ symmetry by the nonlocal dipolar interaction term is closely tied to the emergence of quantum coherence and many-body correlations. In the thermal regime, the measured breathing mode frequency remains consistent with

the scale-invariant prediction $\omega_B = 2\omega_t$ (see empty circles in Fig. 2). However, significant deviations from this value consistently coincide with the onset of strong quantum fluctuations. This is evidenced by the growing discrepancy between the MCTDHB calculation and the GPE predictions. Notably, we are able to resolve this effect experimentally at 90° (see Fig. 3).

In this perspective, the breathing mode frequency measurement can be used to distinguish between different quantum-stabilized phases due to their distinctive physical properties [46, 48], thus paving the way for studying 2D supersolids in a weakly-interacting dilute dipolar gas. The breaking of scale invariance can also be of interest from the perspective of cosmology. As suggested in [69, 70], the scale invariance in a quasi-2D dipolar gas equipped with roton spectrum can validate different possible cosmology models in a scale that is unapproachable by observation, thus opening the possibility of using quasi-2D dipolar gases as the analog cosmology simulator [71, 72].

Methods

Preparation of a strongly dipolar gas of ^{166}Er in a quasi-2D trap In this experiment, we prepare a quasi-2D sample of ^{166}Er using a red-detuned laser sheet and an optical dipole trap [11, 73]. The sheet beam generates tight vertical confinement with a typical trap frequency of $\omega_z = 2\pi \times 1100$ Hz. With a typical atom number of $N \approx 2.8 \times 10^4$, the sample reaches a temperature of $T \approx 50$ nK. The chemical potential μ remains below 30 nK, depending on the dipolar angle, thereby satisfying the quasi-2D criterion $\mu < \hbar\omega_z \sim T$. The radial confinement in the x-y plane is provided by the optical dipole trap. We control the dipole orientation by applying an external magnetic field in the y-z plane. θ denotes the angle between the dipole orientation and the z-axis.

Scale invariance in 2D In the absence of the trap, conformal symmetry is a consequence of the scaling behavior of the mean-field interaction energy [53],

$$E_{\text{interaction}} = E_{\text{contact}} \propto \tilde{g}_0 \int n(r)^2 dr^2, \quad (3)$$

where $n(r)$ is the 2D density and \tilde{g}_0 the dimensionless interaction strength g_0 . Due to its dimensionless nature \tilde{g}_0 does not change by a spatial rescaling of the physical system. In other words, the action $\int dt \{T + E_{\text{contact}}\}$, where T is the total kinetic energy of the gas, remains invariant under the scaling transformation $r \rightarrow \lambda r, t \rightarrow \lambda^2 t$. However, scale invariance only holds at the semiclassical level. Upon the inclusion of quantum fluctuations one realizes that a contact potential is ill-defined in 2D and a regularized interaction potential has to be introduced to describe the 2D gas [74]. The regularization naturally leads to the emergence of a bound state breaking scaling invariance [55]. This phenomenon, known as quantum anomaly, results in an upward shift of the breathing mode frequency with respect to the semiclassical value $2\omega_t$, where ω_t is the frequency of the trap.

Breathing mode measurements We excite the breathing mode by quenching the power of the radial trap, as illustrated in Fig. 1c. The cloud is then allowed to evolve in the trap for varying hold times before being imaged along the z-axis. From the in-situ density profile, we characterize the breathing mode by the average cloud

width $\sigma_r = \sqrt{\sigma_x \sigma_y}$, where σ_x and σ_y are the cloud widths along the two axes, obtained from a 2D Gaussian fit [56]. We perform a damped sinusoidal fit to the oscillation of σ_r to extract the breathing mode frequency ω_B . The typical amplitude of the breathing mode ranges from 6% to 14% of the equilibrium cloud width. Each data point represents an average over 3-6 experimental realizations. Due to residual optical power from the sheet beam within the 2D plane, the trap exhibits a typical anisotropy of $\delta_T = |\omega_y/\omega_x - 1| = 5 \sim 10\%$, which varies as a result of the trap drift. In the contact gas, this level of anisotropy is expected to induce a slight up-shift of the breathing frequency on the order of 0.7% relative to $2\omega_t$ [41, 56].

MCTDHB calculations Within the MCTDHB framework, the many-body wave function is represented as a superposition of permanents constructed from the non-interacting single-particle orbitals, whose amplitudes are variationally optimized to minimize the total energy [75]. By increasing the number M of orbitals, one can, in principle, describe quantum many-body systems in the strongly correlated regime. However, due to the high computational cost of large- M calculations, typical analyses are restricted to $M \gtrsim 2$. We adopt the same approach, restricting our analysis to the cases $M = 1$ (corresponding to the standard GPE) and $M = 2$, which has already proven effective in capturing the dynamics of Bose gases with modulated interactions [76]. To account for anisotropic dipolar interactions in two dimensions, we have extended and modified the publicly available MCTDH-X code [77–79] accordingly. The short-range singularity of the anisotropic dipolar potential is addressed via a regularization scheme [56]. Following the many-body simulations, breathing mode frequencies are extracted from the oscillation period of the collective kinetic energy.

Acknowledgement We acknowledge helpful discussions with Qi Zhou, Tin-Lun Ho and Chengdong He. This work has been supported by the RGC (RFS2122-6S04,C4050-23G). This research was also funded by the Swiss National Science Foundation (SNSF) grant numbers 200021 207537 and 200021 236722 and the Swiss State Secretariat for Education, Research and Innovation (SERI). GBJ acknowledges support from the Gordon and Betty Moore Foundation, grant DOI 10.37807/GBMF13794.

[1] P. C. Hohenberg, Existence of long-range order in one and two dimensions, *Physical Review* **158**, 383 (1967).

[2] V. Berezinskii, Destruction of long-range order in one-dimensional and two-dimensional systems possessing a continuous symmetry group. ii. quantum systems, *Sov. Phys. JETP* **34**, 610 (1972).

[3] J. M. Kosterlitz and D. J. Thouless, Long range order and metastability in two dimensional solids and superfluids (application of dislocation theory), *Journal of Physics C: Solid State Physics* **5**, L124 (1972).

[4] Z. Hadzibabic, P. Krüger, M. Cheneau, B. Battelier, and J. Dalibard, Berezinskii–kosterlitz–thouless crossover in a trapped atomic gas, *Nature* **441**, 1118 (2006).

[5] R. Desbuquois, L. Chomaz, T. Yefsah, J. Léonard, J. Beugnon, C. Weitenberg, and J. Dalibard, Superfluid behaviour of a two-dimensional bose gas, *Nature Physics*

8, 645 (2012).

[6] P. A. Murthy, I. Boettcher, L. Bayha, M. Holzmann, D. Kedar, M. Neidig, M. G. Ries, A. N. Wenz, G. Zürn, and S. Jochim, Observation of the berezinskii-kosterlitz-thouless phase transition in an ultracold fermi gas, *Phys. Rev. Lett.* **115**, 010401 (2015).

[7] C.-L. Hung, X. Zhang, N. Gemelke, and C. Chin, Observation of scale invariance and universality in two-dimensional bose gases, *Nature* **470**, 236 (2011).

[8] T. Yefsah, R. Desbuquois, L. Chomaz, K. J. Günter, and J. Dalibard, Exploring the thermodynamics of a two-dimensional bose gas, *Phys. Rev. Lett.* **107**, 130401 (2011).

[9] R. Desbuquois, T. Yefsah, L. Chomaz, C. Weitenberg, L. Corman, S. Nascimbène, and J. Dalibard, Determination of scale-invariant equations of state without fitting parameters: Application to the two-dimensional bose gas across the berezinskii-kosterlitz-thouless transition, *Phys. Rev. Lett.* **113**, 020404 (2014).

[10] A. Y. Vasiliev, A. Tarkhov, L. Menshikov, P. Fedichev, and U. R. Fischer, Universality of the berezinskii-kosterlitz-thouless type of phase transition in the dipolar xy-model, *New Journal of Physics* **16**, 053011 (2014).

[11] Y. He, Z. Chen, H. Zhen, M. Huang, M. K. Parit, and G.-B. Jo, Exploring the berezinskii-kosterlitz-thouless transition in a two-dimensional dipolar bose gas, *Science Advances* **11**, eadrl2715 (2025).

[12] C. Ticknor, R. M. Wilson, and J. L. Bohn, Anisotropic superfluidity in a dipolar bose gas, *Phys. Rev. Lett.* **106**, 065301 (2011).

[13] S. Yi and H. Pu, Vortex structures in dipolar condensates, *Phys. Rev. A* **73**, 061602 (2006).

[14] B. C. Mulkerin, R. M. W. van Bijnen, D. H. J. O'Dell, A. M. Martin, and N. G. Parker, Anisotropic and long-range vortex interactions in two-dimensional dipolar bose gases, *Phys. Rev. Lett.* **111**, 170402 (2013).

[15] P. Pedri and L. Santos, Two-dimensional bright solitons in dipolar bose-einstein condensates, *Phys. Rev. Lett.* **95**, 200404 (2005).

[16] R. Nath, P. Pedri, and L. Santos, Phonon instability with respect to soliton formation in two-dimensional dipolar bose-einstein condensates, *Phys. Rev. Lett.* **102**, 050401 (2009).

[17] A. Recati and S. Stringari, Supersolidity in ultracold dipolar gases, *Nat. Rev. Phys.* **5**, 735 (2023).

[18] L. Santos, G. V. Shlyapnikov, and M. Lewenstein, Rotomaxon spectrum and stability of trapped dipolar bose-einstein condensates, *Phys. Rev. Lett.* **90**, 250403 (2003).

[19] L. Tanzi, E. Lucioni, F. Famà, J. Catani, A. Fioretti, C. Gabbanini, R. N. Bisset, L. Santos, and G. Modugno, Observation of a dipolar quantum gas with metastable supersolid properties, *Phys. Rev. Lett.* **122**, 130405 (2019).

[20] L. Chomaz, D. Petter, P. Ilzhöfer, G. Natale, A. Trautmann, C. Politi, G. Durastante, R. M. W. van Bijnen, A. Patscheider, M. Sohmen, M. J. Mark, and F. Ferlaino, Long-lived and transient supersolid behaviors in dipolar quantum gases, *Phys. Rev. X* **9**, 021012 (2019).

[21] F. Böttcher, J.-N. Schmidt, M. Wenzel, J. Hertkorn, M. Guo, T. Langen, and T. Pfau, Transient supersolid properties in an array of dipolar quantum droplets, *Phys. Rev. X* **9**, 011051 (2019).

[22] M. A. Norcia, C. Politi, L. Klaus, E. Poli, M. Sohmen, M. J. Mark, R. N. Bisset, L. Santos, and F. Ferlaino, Two-dimensional supersolidity in a dipolar quantum gas, *Nature* **596**, 357 (2021).

[23] T. Bland, E. Poli, C. Politi, L. Klaus, M. A. Norcia, F. Ferlaino, L. Santos, and R. N. Bisset, Two-dimensional supersolid formation in dipolar condensates, *Phys. Rev. Lett.* **128**, 195302 (2022).

[24] Y.-C. Zhang, F. Maucher, and T. Pohl, Supersolidity around a critical point in dipolar bose-einstein condensates, *Phys. Rev. Lett.* **123**, 015301 (2019).

[25] Y.-C. Zhang, T. Pohl, and F. Maucher, Phases of supersolids in confined dipolar bose-einstein condensates, *Phys. Rev. A* **104**, 013310 (2021).

[26] S. M. Roccuzzo, S. Stringari, and A. Recati, Supersolid edge and bulk phases of a dipolar quantum gas in a box, *Phys. Rev. Res.* **4**, 013086 (2022).

[27] B. T. E. Ripley, D. Baillie, and P. B. Blakie, Two-dimensional supersolidity in a planar dipolar bose gas, *Phys. Rev. A* **108**, 053321 (2023).

[28] C. Mishra and R. Nath, Dipolar condensates with tilted dipoles in a pancake-shaped confinement, *Phys. Rev. A* **94**, 033633 (2016).

[29] R. Bombin, J. Boronat, and F. Mazzanti, Dipolar bose supersolid stripes, *Phys. Rev. Lett.* **119**, 250402 (2017).

[30] C. Staudinger, D. Hufnagl, F. Mazzanti, and R. E. Zillich, Striped dilute liquid of dipolar bosons in two dimensions, *Phys. Rev. A* **108**, 033303 (2023).

[31] A. N. Aleksandrova, I. L. Kurbakov, A. K. Fedorov, and Y. E. Lozovik, Density-wave-type supersolid of two-dimensional tilted dipolar bosons, *Phys. Rev. A* **109**, 063326 (2024).

[32] J. Sánchez-Baena, Tilted dipolar bosons in the quasi-two-dimensional regime: From liquid stripes to droplets, *Phys. Rev. A* **112**, 023310 (2025).

[33] D. Lima, M. Grossklags, V. Zampronio, F. Cinti, and A. Mendoza-Coto, Supersolid dipolar phases in planar geometry: Effects of tilted polarization, *Phys. Rev. A* **111**, 063311 (2025).

[34] M. Wenzel, F. Böttcher, T. Langen, I. Ferrier-Barbut, and T. Pfau, Striped states in a many-body system of tilted dipoles, *Phys. Rev. A* **96**, 053630 (2017).

[35] F. Cinti and M. Boninsegni, Absence of superfluidity in 2d dipolar bose striped crystals, *Journal of Low Temperature Physics* **196**, 413 (2019).

[36] F. Cinti and M. Boninsegni, Comment on “berezinskii-kosterlitz-thouless transition in two-dimensional dipolar stripes”, *Phys. Rev. A* **102**, 047301 (2020).

[37] D. S. Jin, J. R. Ensher, M. R. Matthews, C. E. Wieman, and E. A. Cornell, Collective excitations of a bose-einstein condensate in a dilute gas, *Phys. Rev. Lett.* **77**, 420 (1996).

[38] Z. Z. Yan, Y. Ni, A. Chuang, P. E. Dolgirev, K. Seetharam, E. Demler, C. Robens, and M. Zwierlein, Collective flow of fermionic impurities immersed in a bose-einstein condensate, *Nature Physics* **20**, 1395 (2024).

[39] W. Kao, K.-Y. Li, K.-Y. Lin, S. Gopalakrishnan, and B. L. Lev, Topological pumping of a 1d dipolar gas into strongly correlated prethermal states, *Science* **371**, 296 (2021).

[40] K. Merloti, R. Dubessy, L. Longchambon, M. Olshanii, and H. Perrin, Breakdown of scale invariance in a quasi-two-dimensional bose gas due to the presence of the third dimension, *Phys. Rev. A* **88**, 061603 (2013).

[41] G. De Rosi and S. Stringari, Collective oscillations of a trapped quantum gas in low dimensions, *Phys. Rev. A* **92**, 053617 (2015).

[42] M. Holten, L. Bayha, A. C. Klein, P. A. Murthy, P. M. Preiss, and S. Jochim, Anomalous breaking of scale invariance in a two-dimensional fermi gas, *Phys. Rev. Lett.* **121**, 120401 (2018).

[43] M. Holten, L. Bayha, A. C. Klein, P. A. Murthy, P. M. Preiss, and S. Jochim, Anomalous breaking of scale invariance in a two-dimensional fermi gas, *Phys. Rev. Lett.* **121**, 120401 (2018).

[44] L. Chomaz, S. Baier, D. Petter, M. J. Mark, F. Wächtler, L. Santos, and F. Ferlaino, Quantum-fluctuation-driven crossover from a dilute bose-einstein condensate to a macrodroplet in a dipolar quantum fluid, *Phys. Rev. X* **6**, 041039 (2016).

[45] I. Ferrier-Barbut, M. Wenzel, F. Böttcher, T. Langen, M. Isoard, S. Stringari, and T. Pfau, Scissors mode of dipolar quantum droplets of dysprosium atoms, *Phys. Rev. Lett.* **120**, 160402 (2018).

[46] L. Tanzi, S. Rocuzzo, E. Lucioni, F. Famà, A. Fioretti, C. Gabbanini, G. Modugno, A. Recati, and S. Stringari, Supersolid symmetry breaking from compressional oscillations in a dipolar quantum gas, *Nature* **574**, 382 (2019).

[47] L. Tanzi, J. Maloberti, G. Biagioni, A. Fioretti, C. Gabbanini, and G. Modugno, Evidence of superfluidity in a dipolar supersolid from nonclassical rotational inertia, *Science* **371**, 1162 (2021).

[48] C. S. Chisholm, S. Hirthe, V. B. Makhalov, R. Ramos, R. Vatré, J. Cabedo, A. Celi, and L. Tarruell, Probing supersolidity through excitations in a spin-orbit-coupled bose-einstein condensate (2024), arXiv:2412.13861 [cond-mat.quant-gas].

[49] Z. Huang, K. Y. Lee, C. K. Wong, L. Qiu, B. Yang, Y. Yan, and D. Wang, Probing the hollowing transition of a shell-shaped bec with collective excitation (2025), arXiv:2503.12318 [cond-mat.quant-gas].

[50] L. Pitaevskii, Dynamics of collapse of a confined bose gas, *Physics Letters A* **221**, 14 (1996).

[51] F. Chevy, V. Bretin, P. Rosenbusch, K. W. Madison, and J. Dalibard, Transverse breathing mode of an elongated bose-einstein condensate, *Phys. Rev. Lett.* **88**, 250402 (2002).

[52] E. Vogt, M. Feld, B. Fröhlich, D. Pertot, M. Koschorreck, and M. Köhl, Scale invariance and viscosity of a two-dimensional fermi gas, *Phys. Rev. Lett.* **108**, 070404 (2012).

[53] R. Saint-Jalm, P. C. M. Castilho, E. Le Cerf, B. Bakkali-Hassani, J.-L. Ville, S. Nascimbene, J. Beugnon, and J. Dalibard, Dynamical symmetry and breathers in a two-dimensional bose gas, *Phys. Rev. X* **9**, 021035 (2019).

[54] L. P. Pitaevskii and A. Rosch, Breathing modes and hidden symmetry of trapped atoms in two dimensions, *Phys. Rev. A* **55**, R853 (1997).

[55] M. Olshanii, H. Perrin, and V. Lorent, Example of a quantum anomaly in the physics of ultracold gases, *Phys. Rev. Lett.* **105**, 095302 (2010).

[56] See the supplementary.

[57] A. Patscheider, L. Chomaz, G. Natale, D. Petter, M. J. Mark, S. Baier, B. Yang, R. R. W. Wang, J. L. Bohn, and F. Ferlaino, Determination of the scattering length of erbium atoms, *Phys. Rev. A* **105**, 063307 (2022).

[58] Y. Cai, M. Rosenkranz, Z. Lei, and W. Bao, Mean-field regime of trapped dipolar bose-einstein condensates in one and two dimensions, *Phys. Rev. A* **82**, 043623 (2010).

[59] U. R. Fischer, Stability of quasi-two-dimensional bose-einstein condensates with dominant dipole-dipole interactions, *Phys. Rev. A* **73**, 031602 (2006).

[60] C.-A. Chen and C.-L. Hung, Observation of scale invariance in two-dimensional matter-wave townes solitons, *Phys. Rev. Lett.* **127**, 023604 (2021).

[61] N. Bigagli, W. Yuan, S. Zhang, B. Bulatovic, T. Karman, I. Stevenson, and S. Will, Observation of bose-einstein condensation of dipolar molecules, *Nature* **631**, 289 (2024).

[62] Our next work on thermal dipolar gas(in preparation).

[63] H.-D. Meyer, U. Manthe, and L. S. Cederbaum, The multi-configurational time-dependent Hartree approach, *Chemical Physics Letters* **165**, 73 (1990).

[64] U. R. Fischer, A. U. J. Lode, and B. Chatterjee, Condensate fragmentation as a sensitive measure of the quantum many-body behavior of bosons with long-range interactions, *Phys. Rev. A* **91**, 063621 (2015).

[65] L. Pitaevskii and S. Stringari, Elementary excitations in trapped bose-einstein condensed gases beyond the mean-field approximation, *Phys. Rev. Lett.* **81**, 4541 (1998).

[66] L. Chomaz, Quantum-stabilized states in magnetic dipolar quantum gases (2025), arXiv:2504.06221 [cond-mat.quant-gas].

[67] F. Dalfovo, C. Minniti, and L. P. Pitaevskii, Frequency shift and mode coupling in the nonlinear dynamics of a bose-condensed gas, *Phys. Rev. A* **56**, 4855 (1997).

[68] C. J. Pethick and H. Smith, *Bose-Einstein condensation in dilute gases* (Cambridge university press, 2008).

[69] S.-Y. Chä and U. R. Fischer, Probing the scale invariance of the inflationary power spectrum in expanding quasi-two-dimensional dipolar condensates, *Phys. Rev. Lett.* **118**, 130404 (2017).

[70] S. M. Chandran and U. R. Fischer, Expansion-contraction duality breaking in a planck-scale sensitive cosmological quantum simulator (2025), arXiv:2506.02719 [gr-qc].

[71] Z. Tian, S.-Y. Chä, and U. R. Fischer, Roton entanglement in quenched dipolar bose-einstein condensates, *Phys. Rev. A* **97**, 063611 (2018).

[72] Z. Tian, L. Wu, L. Zhang, J. Jing, and J. Du, Probing lorentz-invariance-violation-induced nonthermal unruh effect in quasi-two-dimensional dipolar condensates, *Phys. Rev. D* **106**, L061701 (2022).

[73] B. Seo, Z. Chen, M. Huang, M. K. Parit, Y. He, P. Chen, and G.-B. Jo, Apparatus for producing a 168er bose-einstein condensate, *Journal of the Korean Physical Society* **82**, 901 (2023).

[74] S. A. Coon and B. R. Holstein, Anomalies in quantum mechanics: The $1/r^2$ potential, *American Journal of Physics* **70**, 513 (2002).

[75] O. E. Alon, A. I. Streltsov, and L. S. Cederbaum, Multiconfigurational time-dependent hartree method for bosons: Many-body dynamics of bosonic systems, *Phys. Rev. A* **77**, 033613 (2008).

[76] J. H. V. Nguyen, M. C. Tsatsos, D. Luo, A. U. J. Lode, G. D. Telles, V. S. Bagnato, and R. G. Hulet, Parametric excitation of a bose-einstein condensate: From faraday waves to granulation, *Phys. Rev. X* **9**, 011052 (2019).

[77] P. Molignini, S. Dutta, and E. Fasshauer, Many-body quantum dynamics with MCTDH-X, *SciPost Physics Lecture Notes* **94** (2025).

[78] R. Lin, P. Molignini, L. Papariello, M. C. Tsatsos, C. Lévéque, S. E. Weiner, E. Fasshauer, R. Chitra, and A. U. J. Lode, MCTDH-X: The multiconfigurational time-dependent hartree method for indistinguishable particles software, *Quantum Science and Technology* **5**, 024004 (2020).

[79] A. U. J. Lode, M. Tsatsos, E. Fasshauer, R. Lin, L. Papariello, P. Molignini, C. Lévéque, S. Weiner, M. Büttner, J. Xiang, S. Dutta, D. Ortuño-Gonzalez, Y. Bilinskaya, M. Eder, and L. Fichte, MCTDH-X: The time-dependent multiconfigurational hartree method for indistinguishable particles (software), <https://gitlab.com/the-mctdh-x-repository/mctdh-x-releases> (2025), gitLab repository.

Supplementary: Breaking of scale invariance in a strongly dipolar 2D Bose gas

Haoting Zhen,^{1,*} Yifei He,^{1,*} Sampriti Saha,² Mithilesh K. Parit,¹
Mingchen Huang,¹ Nicolò Defenu,² and Gyu-Boong Jo^{3,4,1,†}

¹*Department of Physics, The Hong Kong University of Science and Technology, Clear Water Bay, Kowloon, Hong Kong*

²*Institut für Theoretische Physik, ETH Zürich, Wolfgang-Pauli-Str. 27 Zürich, Switzerland.*

³*Department of Physics and Astronomy, Rice University, Houston, TX, USA*

⁴*Smalley-Curl Institute, Rice University, Houston, TX, USA*

(Dated: October 27, 2025)

I. EXPERIMENT DETAILS

We generate the quasi-2D dipolar gas using the same procedure described in our previous work [1]. We utilize two image systems to characterize the sample. One is a low-resolution side-image system which images the sample after 16ms time-of-flight (TOF) on the x-z plane. We extract the atom number and temperature of the sample by performing a bimodal fitting on the TOF images. The second image system is built based on a NA=0.28 objective, which collects the insitu density of the sample on the x-y plane. We use this top-down high-resolution image system to measure the motion of the sample on the quasi-2D x-y plane from which we extract the frequencies of the dipole modes and the breathing mode.

Besides estimating the 2D chemical potential by Eq 6, we can extract the chemical potential by fitting the insitu density profile [1]. We fit the thermal tail of the azimuthal average profile of $\theta = 0^\circ$ sample, which admits the least anisotropy generated by magnetostriction effect [2]. The 2D chemical potential is below 30 nK, which qualitatively matches with the result in Fig S3.

II. EXTRACTING THE TRAP FREQUENCY

We measure the trap frequency by extracting the frequency of the dipole mode excited by the quench of radial trap. The dipole mode can be characterized by the oscillatory motion of the cloud center after the quench. Since the trap principal axes do not align with the camera axes, the oscillation in the camera frame is a composition of the sinusoidal oscillations along two trap principal axes, which can be modeled by [3],

$$\begin{pmatrix} x \\ y \end{pmatrix} = \begin{pmatrix} \cos \alpha & -\sin \alpha \\ \sin \alpha & \cos \alpha \end{pmatrix} \begin{pmatrix} \bar{x} \\ \bar{y} \end{pmatrix}. \quad (1)$$

(x, y) and (\bar{x}, \bar{y}) are coordinates in the camera frame and trap frame. α is the angle between the camera axes and trap principal axes. The frequency of the dipole modes extracted in the camera frame may systematically deviate from the real trap frequency. To find α , we perform

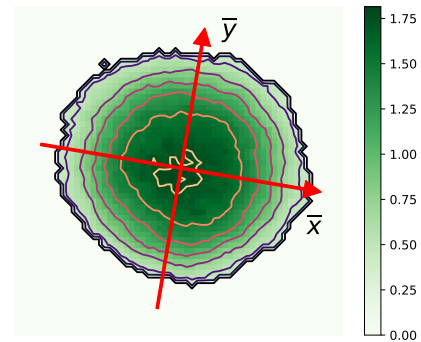


FIG. S1. The trap principal axes extracted from the search. Two red arrows denote the direction of the trap principal axes extracted from the search. The background shows the averaged insitu density of $\theta = 0^\circ$ sample. The contour lines are shown as a guide to the eye. The colorbar denotes the optical density.

a search between $[-\pi/2, \pi/2]$ and determine α that maximizes the fitting quality R^2 of a undamped cosine fit. To validate this search, we compare the direction of the trap principal axes with the density profile of a static 2D sample with $\theta = 0^\circ$, as shown in Fig S1. In this case, the DDIs is isotropically repulsive in the 2D plane, which diminishes the magnetostriction effect that deviates the sample distribution from the trap geometry [2]. The trap principal axes match well with the shape of the example profile, which proves the validity of the search for α . From the oscillation frequencies of \bar{x} and \bar{y} , ω_{dx} and ω_{dy} , we extract the trap frequencies along principal axes as $\omega_{x,y} \equiv \omega_{dx,dy}$. The average trap frequency is computed as $\omega_t = \sqrt{\omega_x \omega_y}$.

We employ a resampling method to evaluate the fitting uncertainty [4]. This method randomly selects a portion of the data points for multiple times and performs a fitting on each selected subset. The uncertainty is represented by the standard deviation of these fitting results. In our work, we resample 80% of the dataset for 1000 times to generate the corresponding fitting uncertainty. Same analysis applies to the extraction of breathing frequency ω_B , explained in the next section.

Due to the daily fluctuation of the optical traps, we observe a fluctuation in ω_t between different data, which

* These authors contributed equally.

† email: gbj@rice.edu

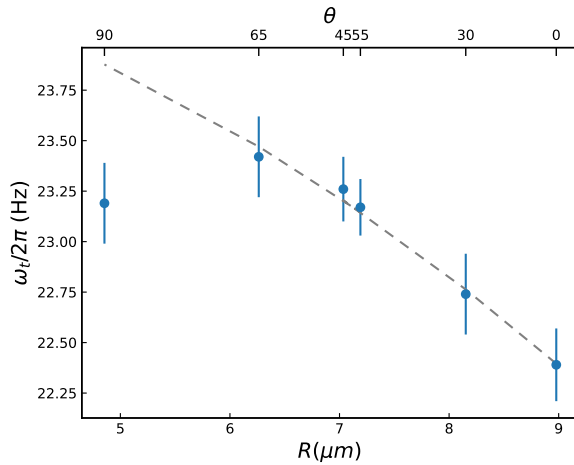


FIG. S2. The trap frequency ω_t with different dipole orientation θ and sample Gaussian width R . The grey dashed line shows the fitting based on the anharmonicity estimate from the sample size [5]. The error bars represent 2σ fitting error.

does not affect the evaluation of the breathing ratio ω_B/ω_t since we simultaneously extract ω_t and ω_B for each data point. For the data with similar trapping, we observe a systematic shift of ω_t with different dipole orientation θ , which we attribute to the anharmonicity arise from the finite sample size [5]. Specifically, if the sample size is smaller than the gaussian beam waist of the optical trap, the optimal trap frequency ω_t is expected to demonstrate a quadratic relationship with the sample size. In Fig S2, we plot ω_t with respect to the Gaussian width R of the average profile of samples with different θ . When θ increases, the effective local interaction decreases, which causes the shrink of sample size, resulting in an increasing ω_t . The measured ω_t matches well with this quadratic model except the one with $\theta = 90^\circ$. We attribute this deviation to the fluctuation of trapping.

III. TRAP ANISOTROPY

Due to the residual radial potential of the tight-confining sheet beam, the radial trap is anisotropic. The trap frequency anisotropy $\delta_t = |\omega_y/\omega_x - 1|$ is ranging from $3 \sim 14\%$, which varies due to the drift of optical potentials. This anisotropy of trap is expected to produce an effect on the breathing frequency, since it induces a coupling between the breathing mode and a quadrupole mode. In a 2D weakly-interacting contact gas, the breathing frequency is given by [6],

$$\omega_B = \sqrt{\frac{3(\omega_x^2 + \omega_y^2)}{2} + \frac{\sqrt{9(\omega_x^2 + \omega_y^2)^2 - 32\omega_x^2\omega_y^2}}{2}}. \quad (2)$$

In the isotropic case $\omega_x = \omega_y = \omega_t$, the ratio $\omega_B/\omega_t = 2$ reflects the $SO(2, 1)$ symmetry. With $\delta_t = 0.1$, the ratio $\omega_B/\omega_t \approx 2.014$ upshifts for around 0.7%. We conclude that the upshift of breathing frequency from the trap anisotropy is small compared to the upshift caused by nonlocal DDIs.

IV. CHARACTERIZING THE BREATHING BEHAVIOR

To characterize the breathing mode excited in the samples, we observe the oscillation of the sample size, represented by its average width $\sigma_r = \sqrt{\sigma_x\sigma_y}$. σ_x and σ_y is the sample width along X and Y axis, generated by performing a 2D Gaussian fitting on the sample profile at each hold time.

We applied a damped cosine fitting to extract the breathing frequency ω_B from the oscillation of σ_r , which can be modeled by [4],

$$\sigma_r(t) = A_0 e^{-k_1 t} \cos(\omega_B t + \phi) + k_2 t + c, \quad (3)$$

where ϕ is a constant phase, k_1 is the damping rate of the breathing mode and k_2 captures the change of sample size caused by heating or atom loss during the holding period. The relative breathing amplitude is defined as A_0/c .

While the trap frequency ω_t has an average anisotropy δ_t of around 8%, we observe small anisotropy in the breathing frequency along x and y axis, extracted from the oscillation of σ_x and σ_y , which is defined as $\delta_B = |\omega_{b,y}/\omega_{b,x} - 1|$ where $\omega_{b,x}$ and $\omega_{b,y}$ are the oscillation frequency of σ_x and σ_y . This is consistent with the hydrodynamic property of condensate where the interaction between atoms result in a phase-lock between the compressional behavior along two axis [5, 7].

V. DETAILS OF THE GPE SIMULATION

In the deep superfluid regime where the system can be describable by classical field theory, we examine the dipolar Gross-Pitaevskii equation (dGPE) with dipole-dipole interactions (DDI) in a quasi-2D harmonic trapping system at the mean-field level [8]. We incorporate DDI into the momentum space and get

$$i\hbar\partial_t\psi_{2D}(x, y, t) = \left\{ -\frac{\hbar^2}{2m}\nabla^2 + V(x, y) + \int \frac{d\mathbf{k}}{(2\pi)^2} e^{ikr \cos \phi_k} \left[g_{\text{eff}} + 3g_{dd}F_d\left(\frac{kl_z}{\sqrt{2}}\right) \right] n(\mathbf{k}) \right\} \psi_{2D}(x, y, t), \quad (4)$$

where

$$F_d(x) = xe^{x^2} \text{erfc}(x)(-\cos^2 \theta + \sin^2 \theta \cos^2 \phi_k), \quad (5)$$

where $g_{\text{eff}} = \frac{4\pi\hbar^2}{m}[(a_s + a_{dd}(3\cos^2 \theta - 1)]$ is the local coupling strength, $g_{dd} = \frac{4\pi\hbar^2}{m}a_{dd}$ is the 2D dipolar coupling strength, erfc is the complementary error function, ϕ_k is the angle between k and the projection of dipole orientation on the 2D plane, and $V(x, y)$ is the external harmonic potential. To calculate the breathing frequency, we solve the time-dependent GPE with GPElab [9, 10] after a quench of the radial trap frequency. To estimate the local interaction and nonlocal interaction in the condensates, we first solve the ground state static density profile through imaginary time propagation, then use the close form of nonlocal interaction given by [8] to calculate the nonlocal interaction energy. When the g_{eff} becomes close to or below zero at large θ and ϵ_{dd} , the system enters the mean-field unstable regime and dGPE fails to give stable oscillation behavior.

VI. BREATHING MODE IN THE 2D-3D CROSSOVER REGIME

DDIs are not the only source that breaks the scale invariance in this experiment. In a quasi-2D quantum gas, the effect of a small portion of excited atoms along the tightly confined direction is known to decrease the breathing mode frequency from standard value [5, 11, 12]. To evaluate this influence of the third dimension, we vary the vertical confinement energy $\hbar\omega_z$ and measure ω_B of the samples with $\theta = 0^\circ$ and $\epsilon_{dd} = 0.98$. The 2D chemical potential μ_{2D} is estimated to quantify this effect [13],

$$\mu_{2D} = 2\hbar\omega_t \sqrt{\frac{N_0 a_{\text{eff}}}{\sqrt{2\pi} l_z}}, \quad (6)$$

where N_0 is the condensate atom number.

As shown in Fig. S3, our measurement qualitatively matches the theoretical model [11]. With the maximal trapping power, ω_B deviates from the 3D limit $\omega_B = 1.83\omega_t$ [6], indicating the quasi-2D nature of our dipolar samples. Since a_{eff} decreases with larger θ , μ_{2D} decreases when dipoles rotate towards the 2D plane, which reduces the effect of the third dimension. We attribute the deviation from the theory to the finite temperature effect [5, 6] and the uncertainty of the μ_{2D} estimation.

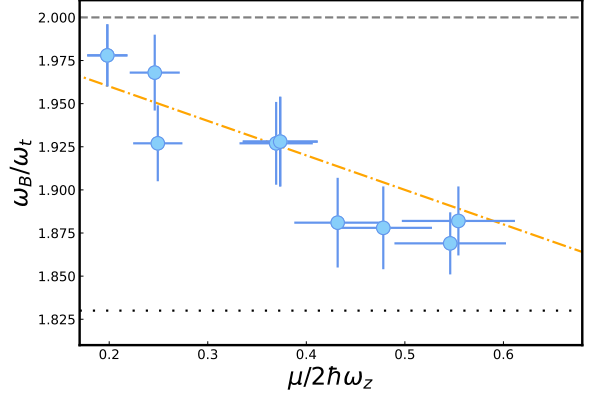


FIG. S3. The breathing mode frequencies versus the vertical confinement energy. The orange dashed line represents the theoretical prediction [11]. The dashed and dotted lines represent the prediction in the 2D and 3D limit [6]. The error bars represent 95% confident interval.

VII. DETAILS OF SIMULATIONS USING MCTDH

As the role of DDI grows in the experimental measurement a larger contribution of quantum fluctuations occurs, demonstrated by increasingly large deviation from the semiclassical GPE prediction. In order to partially describe the rise of strong quantum fluctuations, we implement the Multi-Configurational Time-Dependent Hartree method for Bosons (MCTDHB) [14, 15], to solve the time-dependent (TDSE) and time-independent Schrödinger equations (TISE) for our quasi-2D dipolar system.

Instead of assuming condensation of all the bosons into a single orbital, in this framework, a multi-orbital configuration is considered. In MCTDHB, the ansatz expands the many-body state into a set of M time-dependent single-particle orbitals $\phi_j(\mathbf{r}, t)$ with occupation number n_j , such that $\sum_{j=1}^M n_j = N$. The many-body wavefunction can therefore be written as a superposition of time-dependent permanents [14, 15],

$$|\Psi(t)\rangle = \sum_{n_j} A_{n_1, \dots, n_M}(t) |n_1, \dots, n_M; t\rangle, \quad (7)$$

where,

$$\begin{aligned} |n_1, \dots, n_M; t\rangle &= \frac{\prod_{j=1}^M (\hat{a}_j^\dagger(t))^{n_j}}{\sqrt{n_1! \cdots n_M!}} |0\rangle, \\ \hat{a}_j^\dagger(t) &= \int d\mathbf{r} \phi_j(\mathbf{r}, t) \hat{\Psi}^\dagger(\mathbf{r}) \end{aligned} \quad (8)$$

where $\phi_j(\mathbf{r}, t)$ are the dynamically optimized single-particle orbitals. In the $M \rightarrow \infty$ limit, the method captures the exact dynamics of the system, since the non-interacting permanent basis is a complete basis. Of course, in any practical numerical computation the sum has to be truncated to a finite number of orbitals M . The time-dependent coefficients $A_{n_1, \dots, n_M}(t)$ and the orbitals $\phi_j(\mathbf{r}, t)$ are the variational parameters which are determined by exploiting the Dirac–Frenkel principle [14–16].

By allowing population of multiple, dynamically optimized orbitals, the ansatz itself takes into account the correlations between orbitals and coherent superpositions between configurations, hence capturing many-body quantum effects like fragmentation, depletion, and entanglement, beyond the mean-field Gross–Pitaevskii description, which is recovered at $M = 1$.

MCTDHB simulations are carried out for a perfect 2D plane and ignore the tight transverse confinement ω_z , ensuring that confounding effects from the finite depth of the cloud are not included. We measure distances in units of the 2D confinement $l_x = \sqrt{\frac{\hbar}{m\omega_x}}$, where ω_x is the trap frequency along the x -axis. The parameters are rescaled as, $\rho \rightarrow l_x \rho$, $t \rightarrow t/\omega_x$. The many-body Hamiltonian in harmonic oscillator units can hence be expressed as,

$$\begin{aligned} \hat{H} = & \left[-\frac{1}{2} \nabla_i^2 + \frac{1}{2} (x_i^2 + \frac{\omega_y^2}{\omega_x^2} y_i^2) \right] + \left[g_{2D} \delta^{(2)}(\boldsymbol{\rho}_i - \boldsymbol{\rho}_j) \right. \\ & \left. + V_{2D}^{\text{reg}}(\boldsymbol{\rho}_i - \boldsymbol{\rho}_j) \right], \end{aligned} \quad (9)$$

with $\boldsymbol{\rho} = (x, y)$ denoting planar coordinates. In the quasi-2D limit the contact coupling takes the form $g_{2D} = \frac{4\pi a_s}{\sqrt{2\pi\gamma} l_x}$ (in our dimensionless harmonic-oscillator units), where a_s is the s -wave scattering length and $\gamma = \omega_x/\omega_z$, ratio of the trap frequencies along x and z directions.

In order to project the dipolar interactions to the 2D plane, one has to first consider the 3D expression [17, 18],

$$V_{dd}(\mathbf{r}_1 - \mathbf{r}_2) = \frac{C_{dd}}{4\pi} \frac{1 - 3 \cos^2 \theta}{|\mathbf{r}_1 - \mathbf{r}_2|^3}, \quad (10)$$

where $C_{dd} = \mu_0 \mu^2$ signifies the dipolar strength and θ is the relative angle between the two dipoles. In the quasi-two-dimensional regime, harmonic confinement along z is strong enough such that the motion freezes into the ground state $\Phi_0(z)$, making the wavefunction separable. Hence, the effective interaction can be obtained by integrating out the z direction [19],

$$V_{2D}(\rho) = \int dz dz' |\Phi_0(z)|^2 V_{dd}(\rho, z - z') |\Phi_0(z')|^2. \quad (11)$$

To handle the short-distance divergence of the DDI in real space, we introduce a short-range cut-off. The regularised potential can be expressed as follows:

$$V_{2D}^{\text{reg}}(\rho) = \begin{cases} 0, & \rho < \frac{\ell_z}{2}, \\ V_{2D}(\rho), & \rho \geq \frac{\ell_z}{2} \end{cases} \quad (\rho = |\rho|). \quad (12)$$

Here, ℓ_z is the oscillator length of the tight z -confinement. This cutoff helps us to overcome the unphysical singularity while maintaining the long-range anisotropic dipolar tail, which is responsible for the collective physics and low-energy scattering properties of the potential.

In our simulations, we stick to 2 orbitals, since, the occupation of first excited state is very low ($n_1/n_0 \ll 1$), we do not expect substantial corrections on addition of further orbitals. $M = 2$ allows us to capture the leading quantum correlations, without being computationally expensive [20, 21]. The ansatz then reduces to

$$|\Psi(t)\rangle = \sum_{n=0}^N A_n(t) \frac{(\hat{a}_1^\dagger(t))^n (\hat{a}_2^\dagger(t))^{N-n}}{\sqrt{n!(N-n)!}} |0\rangle, \quad (13)$$

leading to coupled equations of motion for $A_n(t)$ and for the orbitals ϕ_1, ϕ_2 . We set the atom number to $N = 2000$ and re-scale the scattering length and dipolar lengths accordingly. Unlike GPE, for $M > 1$ the number of particles affect the numerical stability of the MCTDHB [22]. In practice, $N \sim 10^3$ ensures stable convergence of two-orbital ($M = 2$) calculations.

We obtain the many-body ground state by evolving Eq. (13) (orbitals and coefficients) in imaginary time $t = i\tau$. We claim the results have converged, and hence ground state has been obtained, when the total energy and the natural-orbital occupations become stationary within the defined tolerance range,

$$|E^{(k)} - E^{(k-1)}| < \delta\varepsilon_E, \quad |n_\alpha^{(k)} - n_\alpha^{(k-1)}| < \delta\varepsilon_n, \quad (14)$$

where n_α denotes the occupation of the α -th natural orbital, and k denotes the index of the k -th time step (or iteration). In our computations we use $\delta\varepsilon_n = 10^{-12}$ and $\delta\varepsilon_E = 10^{-8}$. Employing the ground state, obtained via imaginary time propagation, as the initial condition, we then implement real-time propagation of the coupled MCTDHB equations to study the breathing dynamics.

The non-linear coupled equations for the orbitals are integrated using the Runge–Kutta method of order 8. At the same time, for the coefficient part, the linear coupled equations are integrated by implementing the Davidson diagonalization for imaginary time evolution, while the MCTDH short-iterative Lanczos (MCS) propagator is used for real time propagation. Spatial discretization is performed with a discrete variable representation (DVR). The MCTDH-X package [23, 24] is used for both ground-state relaxations and real-time evolutions. We have extended and modified the available MCTDH-X code [25] to incorporate the regularized anisotropic dipolar interactions in two dimensions, which enables us to perform the

simulation of quantum many-body effects in these systems.

To extract the radial breathing frequency, we monitor the oscillation of kinetic energy after the quench and determine its period. We then normalize this frequency by

the geometric average of the radial trapping frequency $\omega_R = \sqrt{\omega_x \omega_y}$. The resulting frequencies, together with experimental data, are presented in the main text; within uncertainties, the theory shows good agreement across the parameter range.

[1] Y. He, Z. Chen, H. Zhen, M. Huang, M. K. Parit, and G.-B. Jo, Exploring the berezinskii-kosterlitz-thouless transition in a two-dimensional dipolar bose gas, *Science Advances* **11**, eadr2715 (2025).

[2] L. Chomaz, I. Ferrier-Barbut, F. Ferlaino, B. Laburthe-Tolra, B. L. Lev, and T. Pfau, Dipolar physics: a review of experiments with magnetic quantum gases, *Reports on Progress in Physics* **86**, 026401 (2022).

[3] R. J. Fletcher, *Bose-Einstein condensation and superfluidity in two dimensions*, Ph.D. thesis, University of Cambridge (2015).

[4] W. Kao, K.-Y. Li, K.-Y. Lin, S. Gopalakrishnan, and B. L. Lev, Topological pumping of a 1d dipolar gas into strongly correlated prethermal states, *Science* **371**, 296 (2021).

[5] M. Holten, L. Bayha, A. C. Klein, P. A. Murthy, P. M. Preiss, and S. Jochim, Anomalous breaking of scale invariance in a two-dimensional fermi gas, *Phys. Rev. Lett.* **121**, 120401 (2018).

[6] G. De Rosi and S. Stringari, Collective oscillations of a trapped quantum gas in low dimensions, *Phys. Rev. A* **92**, 053617 (2015).

[7] E. Vogt, M. Feld, B. Fröhlich, D. Pertot, M. Koschorreck, and M. Köhl, Scale invariance and viscosity of a two-dimensional fermi gas, *Phys. Rev. Lett.* **108**, 070404 (2012).

[8] Y. Cai, M. Rosenkranz, Z. Lei, and W. Bao, Mean-field regime of trapped dipolar bose-einstein condensates in one and two dimensions, *Phys. Rev. A* **82**, 043623 (2010).

[9] X. Antoine and R. Duboscq, Gpelab, a matlab toolbox to solve gross-pitaevskii equations i: Computation of stationary solutions, *Computer Physics Communications* **185**, 2969 (2014).

[10] X. Antoine and R. Duboscq, Gpelab, a matlab toolbox to solve gross-pitaevskii equations ii: Dynamics and stochastic simulations, *Computer Physics Communications* **193**, 95 (2015).

[11] K. Merloti, R. Dubessy, L. Longchambon, M. Olshanii, and H. Perrin, Breakdown of scale invariance in a quasi-two-dimensional bose gas due to the presence of the third dimension, *Phys. Rev. A* **88**, 061603 (2013).

[12] M. Holten, L. Bayha, A. C. Klein, P. A. Murthy, P. M. Preiss, and S. Jochim, Anomalous breaking of scale invariance in a two-dimensional fermi gas, *Phys. Rev. Lett.* **121**, 120401 (2018).

[13] K. Merloti, R. Dubessy, L. Longchambon, A. Perrin, P.-E. Pottie, V. Lorent, and H. Perrin, A two-dimensional quantum gas in a magnetic trap, *New Journal of Physics* **15**, 033007 (2013).

[14] O. E. Alon, A. I. Streltsov, and L. S. Cederbaum, Multiconfigurational time-dependent hartree method for bosons: Many-body dynamics of bosonic systems, *Phys. Rev. A* **77**, 033613 (2008).

[15] A. I. Streltsov, O. E. Alon, and L. S. Cederbaum, General variational many-body theory with complete self-consistency for trapped bosonic systems, *Phys. Rev. A* **73**, 063626 (2006).

[16] M. H. Beck, A. Jäckle, G. A. Worth, and H.-D. Meyer, The multiconfiguration time-dependent Hartree (MCTDH) method: A highly efficient algorithm for propagating wavepackets, *Physics Reports* **324**, 1 (2000).

[17] J. Stuhler, A. Griesmaier, T. Koch, M. Fattori, T. Pfau, S. Giovanazzi, P. Pedri, and L. Santos, Observation of dipole-dipole interaction in a degenerate quantum gas, *Phys. Rev. Lett.* **95**, 150406 (2005).

[18] J. Sánchez-Baena, Tilted dipolar bosons in the quasi-two-dimensional regime: From liquid stripes to droplets, *Phys. Rev. A* **112**, 023310 (2025).

[19] C. Ticknor, Quasi-two-dimensional dipolar scattering, *Phys. Rev. A* **81**, 042708 (2010).

[20] J. H. V. Nguyen, M. C. Tsatsos, D. Luo, A. U. J. Lode, G. D. Telles, V. S. Bagnato, and R. G. Hulet, Parametric excitation of a bose-einstein condensate: From faraday waves to granulation, *Phys. Rev. X* **9**, 011052 (2019).

[21] C. Menotti, J. R. Anglin, J. I. Cirac, and P. Zoller, Dynamic splitting of a bose-einstein condensate, *Phys. Rev. A* **63**, 023601 (2001).

[22] I. Březinová, A. U. J. Lode, A. I. Streltsov, O. E. Alon, L. S. Cederbaum, and J. Burgdörfer, Wave chaos as signature for depletion of a bose-einstein condensate, *Phys. Rev. A* **86**, 013630 (2012).

[23] P. Molignini, S. Dutta, and E. Fasshauer, Many-body quantum dynamics with MCTDH-X, *SciPost Physics Lecture Notes* **94** (2025).

[24] R. Lin, P. Molignini, L. Papariello, M. C. Tsatsos, C. Lévéque, S. E. Weiner, E. Fasshauer, R. Chitra, and A. U. J. Lode, MCTDH-X: The multiconfigurational time-dependent hartree method for indistinguishable particles software, *Quantum Science and Technology* **5**, 024004 (2020).

[25] A. U. J. Lode, M. Tsatsos, E. Fasshauer, R. Lin, L. Papariello, P. Molignini, C. Lévéque, S. Weiner, M. Büttner, J. Xiang, S. Dutta, D. Ortuño-Gonzalez, Y. Bilinskaya, M. Eder, and L. Fichte, MCTDH-X: The time-dependent multiconfigurational hartree method for indistinguishable particles (software), <https://gitlab.com/the-mctdh-x-repository/mctdh-x-releases> (2025), gitLab repository.